THE EUROPEAN
PHYSICAL JOURNAL PLUS

A case study of the May 30, 2017, Italian fireball

Albino Carbognani[1,2,a] , D. Barghini[2,3], D. Gardiol[2], M. Di Martino[2],
G. B. Valsecchi[4,5], P. Trivero[6], A. Buzzoni[1], S. Rasetti[2], D. Selvestrel[7], C. Knapic[8],
E. Londero[8], S. Zorba[8], C. A. Volpicelli[2], M. Di Carlo[9], J. Vaubaillon[10], C. Marmo[11],
F. Colas[10], D. Valeri[12,13], F. Zanotti[13], M. Morini[13], P. Demaria[13], B. Zanda[14],
S. Bouley[11], P. Vernazza[15], J. Gattacceca[16], J. L. Rault[17], L. Maquet[10], M. Birlan[10]

[1] INAF-Osservatorio di Astrofisica e Scienza dello Spazio, Via Piero Gobetti, 93/3, 40129 Bologna, Italy
[2] INAF-Osservatorio Astrofisico di Torino, Via Osservatorio 20, 10025 Pino Torinese, TO, Italy
[3] Dipartimento di Fisica, Univ. degli studi di Torino, Turin, Italy
[4] IAPS-INAF, Via Fosso del Cavaliere 100, 00133 Rome, Italy
[5] IFAC-CNR, via Madonna del Piano 10, 50019 Sesto Fiorentino, Italy
[6] Dip. Di Scienze e Innovazione Tecnologica, Univ. del Piemonte Orientale, Viale Teresa Michel, 11,
  15121 Alessandria, Italy
[7] INAF-Osservatorio Astronomico di Padova, Vicolo dell'Osservatorio 5, 35122 Padua, Italy
[8] INAF-Osservatorio Astronomico di Trieste, Via G.B. Tiepolo 11, 34143 Trieste, Italy
[9] INAF-Osservatorio Astronomico d'Abruzzo, Via Mentore Maggini, 64100 Teramo, Italy
[10] IMCCE, Observatoire de Paris, PSL Research University, CNRS, Sorbonne Université s, UPMC, Paris,
  France
[11] GEOPS, Univ. Paris-Sud, CNRS, Univ. Paris-Saclay, Orsay, France
[12] Dipartimento di Ingegneria Civile, Edile ed Ambientale, Univ. La Sapienza, Rome, Italy
[13] Italian Meteor and TLE Network (IMTN), Ferrara, Italy
[14] IMPMC, Muséum National d'Histoire Naturelle, Paris, France
[15] LAM, Institut Pytheas, Marseille, France
[16] CEREGE, Institut Pytheas, Marseille, France
[17] FRIPON, Collaborative Team, Paris, France

Abstract On May 30, 2017, at about 21 h 09 min 17 s UTC a green bright fireball crossed the
sky of northeastern Italy. The fireball path was observed from some all-sky cameras starting
from a mean altitude of 81.1 ± 0.2 km (Lat. $44.369° \pm 0.002°$ N; Long. $11.859° \pm 0.002°$ E)
and extinct at 23.3 ± 0.2 km (Lat. $45.246° \pm 0.002°$ N; Long. $12.046° \pm 0.002°$ E), between
the Italian cities of Venice and Padua. In this paper, on the basis of simple physical models,
we will compute the atmospheric trajectory, analyze the meteoroid atmospheric dynamics,
the dark flight phase (with the strewn field) and compute the best heliocentric orbit of the
progenitor body. Search for meteorites on the ground has not produced any results so far.

1 Introduction

One of the most interesting astronomical phenomena that can be seen in the sky is a
fireball, namely a very bright meteor caused by the impact of a big meteoroid into the

[a] e-mail: albino.carbognani@inaf.it (corresponding author)

atmosphere.[1] Unfortunately, as the events are sporadic and unpredictable, it is not possible to know when you will see the next fireball so we need constant monitoring of the whole sky in order to observe one.

A fireball with absolute mag lower than -17 is called superbolide. For small asteroids of tens of meters in diameter, a superbolide can be brighter than the Sun when seen from the Earth. An example of such an extreme event is the small asteroid of 19.8 ± 4.6 m in diameter exploded at an altitude of about 27 km above the city of Chelyabinsk (Russia) on February 15, 2013, at about 03:20.5 UTC [25].

Often, less cohesive meteoroids during fall are fragmented into several blocks each of which becomes an independent fireball. A similar event occurred for the bolide seen from Peekskill (New York State) on the evening of October 9, 1992, at 23:48 UTC. At a height of about 41.5 km, extensive fragmentation of the meteoroid occurred. The meteorite recovered at Peekskill was subsequently identified as an H6 breccia meteorite [3].

If the meteoroid is large enough and the speed is not too high, a portion of it can survive the atmospheric ablation phase. When the velocity in the atmosphere drops below about 3 km/s, the mass loss and the radiation emission cease and the meteoroid enters the dark flight phase [13]. A process of surface cooling begins, and the trajectory of the body becomes more and more vertical. The impact velocity of the meteoroid on the Earth's surface ranges from 10 to 100 m/s for bodies of mass between 10 g and 10 kg and geocentric speed of about 15 km/s [13]. What remains of the meteoroid on the ground is called a meteorite. Most meteoroids totally disintegrate in the air, and the impact of some fragments with the Earth's surface is rare.

Meteorites are very important because they provide information on the composition and thermal history of asteroids in the early solar system and provide a possible vehicle for the dissemination of water and organic materials. For these reasons, it is important to recover as many meteorites as possible after observation of bright fireball events.

The physical analysis of a fireball event can be ideally divided into four distinct phases:

1. Triangulation between different stations on the ground for the reconstruction of the average fireball trajectory in the atmosphere.
2. Estimate of pre-atmospheric velocity, mean drag/ablation coefficients and mass–section ratio. From pre-atmospheric velocity, correcting it for the Earth's attraction and rotation (with "zenith attraction" method), we can compute the true geocentric velocity.
3. Starting from the terminal point of the luminous path, modeling of the dark flight phase to estimate the area on the ground where to look for possible meteorites (strewn field).
4. Compute the heliocentric velocity from the meteoroid true geocentric velocity and, knowing the position vector of the Earth at the fireball time, compute the meteoroid heliocentric osculating orbit. The knowledge of the heliocentric orbit is important because it allows to go in search of the meteoroid progenitor body.

This is the logical path we will follow in this paper, applied to the Italian fireball of May 30, 2017, which we will also call with the code "country code yyyymmdd," i.e., IT20170530.

2 PRISMA, FRIPON, IMTN and CMN networks

PRISMA[2] network was born in 2016 [19] and means "Prima Rete Italiana per la Sorveglianza sistematica di Meteore e Atmosfera," i.e., First Italian Network for Meteor and Atmosphere

---

[1] According to the IAU definition, a bolide or a fireball is a meteor brighter than absolute visual magnitude -4 (distance of 100 km).

[2] www.prisma.inaf.it.

systematic Surveillance, and is managed by INAF, the Italian National Institute for Astrophysics. The word "first" in the abbreviation of PRISMA indicates the first national network dedicated to fireballs. In Italy, there are also local amatorial networks for observing meteors, and in fact, for the purpose of this paper, we used data from one of them. PRISMA's primary goal is to observe fireballs and recovery any subsequent meteorites while progressively increasing the number of all-sky automatic cameras throughout Italy, so as to have a camera every 80–100 km. As Italy has a surface of 301,338 km^2, we need about 50 cameras to cover the whole country with squares of 80 km side. It is crucial to note that inclusion in the PRISMA network is on a voluntary basis. Anyone can cooperate (universities, research centers, schools, amateur astronomers and so on), but must find funding for the purchase of the station's hardware. At present (Nov 2019), 51 all-sky cameras are available, 37 devices in full working mode and 14 in setup phase (see Fig. 1), whereas on May 2017 only five PRISMA cameras were in operation, mostly in northern Italy.

The PRISMA project is an international European collaboration with the French project FRIPON[3] (Fireball Recovery and InterPlanetary Observation Network), started in 2014 and managed by l'Observatorire de Paris, Muséum National d'Histoire Naturelle, Université Paris-Sud, Université Aix Marseille and CNRS [15]. The hardware (and software) of a PRISMA station is similar to a FRIPON station and consists of a small CCD camera kept at room temperature and equipped with a short focal lens objective in order to have a wide FoV (Field of View). The camera is connected via LAN to a local mini-PC with Linux-Debian operating system and equipped with a mass storage device of about 1 TB.

Acquisition and detection are done on the local mini-PC by open-source software FreeTure,[4] i.e., Free software to capTure meteors [1], developed by the FRIPON team. Acquisition rate is 30 fps, and only bright events with a negative magnitude are recorded. For event detection, FreeTure uses the subtraction of two consecutive frames with a detection threshold. In order to reduce the amount of false positives, before starting a detection FreeTure waits for a third frame with something moving in the FoV. Every time something bright passes through the FoV of the camera, there is a detection and all the images regarding the event, in standard FITS format, are saved in the HDD of the mini-PC that controls the camera. A message is sent to the central FRIPON server, located in the Laboratoire d'Astrophysique de Marseille (LAM), for each local detection. If there is a simultaneous detection in another location, the data are downloaded; if not, the data stay on the local HDD for 2 months before being deleted. The reduction pipeline on LAM is launched for every multiple detection.

Regarding data reduction, every 10 min a calibration image with an exposure time of 5 s is taken from station. In these calibration images, stars up to the apparent mag +4.5 are used for the astrometric calibration of the camera using the pipeline on LAM developed by FRIPON team and based on the software SExtractor and SCAMP.[5] SExtractor is a program that builds a catalog of objects from an astronomical image, while SCAMP reads SExtractor catalogs and, using a star catalog, computes astrometric and photometric solutions for any arbitrary sequence of FITS images in a completely automatic way [4,5]. As an astrometric catalog, SCAMP uses the Tycho 2 star catalog. For the known stars, the accuracy of astrometric calibration is between 100 and 200 arcsec root mean square, more frequently around 150 arcsec.

---

[3] www.fripon.org.

[4] www.github.com/fripon/freeture.

[5] www.astromatic.net/software.

Fig. 1 A map from Google Earth showing the distribution of PRISMA stations on April 2019. Most of the stations are concentrated in northern Italy. Legend: dark dots = working camera; gray/white dots = setup phase

The IMTN[6] (Italian Meteor and TLE Network) is a surveillance network managed by amateur astronomer both for the study of meteors and high-atmosphere phenomena or TLE, Transient Luminous Events. Generally, IMTN stations have a smaller FoV than PRISMA stations, because the camera objective tends to have higher focal lengths, but on the other hand, the images have slightly higher resolution. An observation from a station of the Croatian Meteor Network (CMN) was also collected. The CMN[7] consists of 30 surveillance cameras each having a FoV of 64×48 deg. The cameras monitor most of the night sky over Croatia. See Table 1 and Fig. 2 for more details about the cameras that captured IT20170530. IMTN members normally use commercial software as UFOOrbit given by SonotaCo[8] for the movie capture, the astrometric reduction in the fireballs images and the computation of the trajectory and orbits. As astrometric star catalog IMTN uses the SKYMAP Master Catalog,[9] Version 4, which features an extensive compilation of information on almost 300,000 stars brighter

---

6 www.meteore.forumattivo.com.

7 www.cmn.rgn.hr.

8 www.sonotaco.com.

9 www.tdc-www.harvard.edu/catalogs/sky2k.html.

Table 1 Some technical data about PRISMA, IMTN and CMN stations that observed IT20170530

Name	Lat. N (°)	Long. E (°)	El. (m)	Camera model	FL (mm)	FoV (°)	fps	Scale
PRISMA-Navacchio	43.68320	10.49163	015	Basler A1300gm	1.2	223 × 166	30	600
PRISMA-Piacenza	45.03538	09.72503	077	Basler A1300gm	1.2	223 × 166	30	600
PRISMA-Rovigo	45.08167	11.79505	015	Basler A1300gm	1.2	223 × 166	30	600
IMTN-Casteggio	44.98810	09.12510	238	Mintron MTV-12V6H-EX	4.0	92 × 69	25	430
IMTN-Confreria	44.39590	07.51730	550	Watec 120 N+	4.5	82 × 62	25	385
IMTN-Contigliano	42.41140	12.76820	421	Mintron MTV-12V6H-EX	4.0	92 × 69	25	430
IMTN-Ferrara	44.81760	11.61060	009	Mintron MTV-12V6H-EX	2.6	142 × 106	25	666
CMN-Ciovo (Croatia)	43.51351	16.29545	020	SK1004X	4.0	64 × 48	25	325

From left to right: name, latitude, longitude and elevation over sea level; camera model, objective focal length, approximate field of vision, frame rate and scale of images in arcsec/pixel. In bold type, the stations whose observations were used to compute the fireball trajectory (see text about this choice)
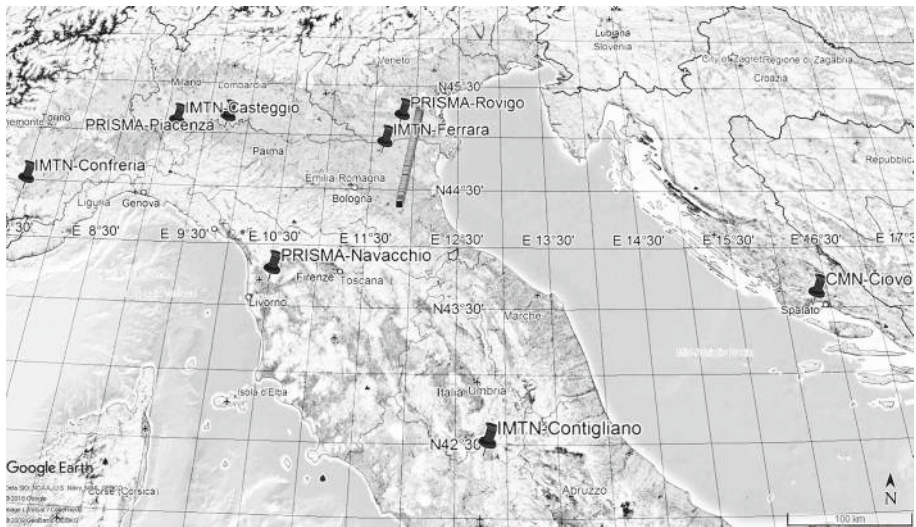
Fig. 2 A Google Earth map showing the position of the stations listed in Table 1 and the fireball trajectory projected on the ground

than 8.0 mag. In this case, the accuracy of astrometric calibration is between 100 and 180 arcsec root mean square.

3 Software packages for fireballs analysis

We did not use the FRIPON astrometric pipeline that we briefly illustrated above for the astrometric reduction in the fireball images. Rather, for the PRISMA team the observation of IT20170530 was a good opportunity to start developing an independent pipeline. In this section, we briefly describe the main software packages available so far.

3.1 Astrometry

The determination of an astrometric solution for all-sky cameras has been already discussed in the literature, from Ceplecha to Borovička [8,9,12]. The astrometric model is based on a parametric description of heavy optical distortions in the radial coordinate due to the lens type [12]. Minor but still significant effects due to the displacement of the optical axis with respect to the zenith direction and camera misalignments are taken into account in a refined model [8,9]. We have implemented this model with IDL (Interactive Data Language)[10] to derive the astrometry of the fireball by means of the IDL-Astro and Markwardt-IDL libraries. On a bright fireball, the position error on a single frame is of the order of 1 arcmin, so that any astrometric inaccuracies introduced by the model become negligible using a set of calibration data spanning a few months of observations. This is not completely true at very low elevation, especially with a degraded point spread function (PSF). Regarding the details about the astrometric reduction technique, see Barghini et al., 2019 [6].

---

10 www.harrisgeospatial.com/SoftwareTechnology/IDL.aspx.

3.2 Physical analysis

Analysis of the astrometry data files from IDL was carried out by writing a software able to run under MATLAB® Release 2015b (MathWorks®, Inc., Natick, Massachusetts, USA).[11] The code has been divided into four main functions concerning trajectory, dynamics model, dark flight (with strewn field) and osculating heliocentric (or barycentric) orbit. In the trajectory function, the preliminary atmospheric path of the fireball was computed as geometric intersection of the best planes containing two stations and the unit vectors of the fireball's observed points [12]. The definitive best fireball trajectory was obtained with observations from $N > 2$ stations simultaneously, using the Borovička method [7]. In this way, the values of the starting and terminal height (H_s and H_t), of the trajectory inclination on the Earth's surface (T_i) and of the azimuth were the fireball came from (A_z) are found. Associated with the heights values, there are also the geographical coordinates, longitude and latitude, respectively, starting (Lo_s, La_s) and terminal (Lo_t, La_t). Following this method, the result about fireball trajectory is always a straight line and it is interesting to note that it is not necessary to have accurate temporal data from all the stations to have geometric triangulation. The analysis software package was called MuFiS (Multipurpose Fireball Software) because it includes triangulation, dynamics, dark flight and orbit functions. We will see the underground physics of the other MuFiS's functions in the next sections, coupled with the IT20170530 analysis.

MuFiS has been verified by applying it to a synthetic fireball with known initial parameters. The synthetic fireball was generated by writing a completely independent software. To be realistic, four trajectories seen from four different stations have been simulated and, on each trajectory, a random uncertainty of 1/100 s over time and 1 arcmin in the position was added. In general, the agreement between the synthetic data and those found by MuFiS is very good, see Table 2 for a comparison between synthetic and MuFiS values. It is interesting to note that if you adopt a drag coefficient value (Γ) different from the one used to generate the synthetic fireball, the triangulation values are the same, but the guess estimated values about the meteoroid mass and diameter change. This happens because the dynamic model fit provides the Γ/D_∞ ratio only, where D_∞ is the meteoroid pre-atmospheric ratio mass/section. Fortunately, the terminal point values from dynamical analysis (height H_{fin}, velocity v_{fin} and acceleration a_{fin}), useful to compute the dark flight phase, are independent from the Γ value as we discussed in Sects. 5 and 6. The adopted dynamic model is discussed in detail in Sect. 5. MuFiS detailed structure will be explained in a next future paper.

4 The fireball atmospheric trajectory

And now let's start with the analysis of the fireball trajectory in the atmosphere. There are 285 position points available from Rovigo, for a total duration of about 9.51 s. Unfortunately, for Piacenza and Navacchio the bolide was very low above the horizon in an area of the focal plane where resolution is very poor. This, combined with the remarkable distance between both cameras and the bolide (roughly 200 km), makes the determination of the bolide position in geocentric coordinates much more difficult. Fortunately, the data from Rovigo are the best of the trio because the fireball passed near the zenith and, thanks to the favorable geographical position, the trajectory terminal point was imaged (see Fig. 3). For these reasons, the triangulation of the fireball trajectory was performed with the data from Rovigo crossed with the data from the IMTN/CMN stations. Data from these stations are good

---

[11] http://www.mathworks.com.

Table 2 Comparison between a synthetic fireball generated by a 3.5-kg meteoroid (supposed to be a chondrite with an average density of 3500 kg/m^3) and ablation coefficient 0.0070 s^2/km^2 that falls into the atmosphere with a pre-atmospheric speed of 21 km/s and the solutions found by MuFiS about triangulation and dynamic model

Quantity	Synthetic ($\Gamma = 0.7$)	MuFiS ($\Gamma = 0.70$)	MuFiS ($\Gamma = 0.58$)	MuFiS ($\Gamma = 0.80$)
H_s (km)	71.0	70.8	70.8	70.8
La_s (N, °)	44.3694	44.3695	44.3695	44.3695
Lo_s (E, °)	11.8594	11.8600	11.8600	11.8600
H_t (km)	21.8	21.9	21.9	21.9
La_t (N, °)	44.7310	44.7310	44.7310	44.7310
Lo_t (E, °)	11.9489	11.9492	11.9492	11.9492
T_i (°)	50	49.8	49.8	49.8
A_z (from north to south, °)	190	190	190	190
v_∞ (km/s)	21.0	20.9	20.9	20.9
σ (s^2/km^2)	0.0070	0.0068	0.0068	0.0068
D_∞ (kg/m^2)	289	281	233	321
d_∞ (m)	0.12	0.12	0.10	0.14
m_∞ (kg)	3.5	3.2	1.8	4.8
D_{fin} (kg/m^2)	173	172	143	197
d_{fin} (m)	0.07	0.07	0.06	0.08
m_{fin} (kg)	0.7	0.7	0.4	1.10
v_{fin} (km/s)	3.0	3.0	3.0	3.0
a_{fin} (km/s^2)	−2.4	−2.4	−2.4	−2.4
H_{fin} (km)	21.8	21.9	21.9	21.9

Note that if you adopt a drag coefficient value (Γ), different from the one used to generate the synthetic fireball, the triangulation values are the same, but the guess estimated values about the meteoroid mass and diameter change. The terminal point values, necessary to compute the dark flight phase, are independent from the Γ value. For details and limits about the adopted dynamic model, see Sect. 5

for geometrical triangulation (i.e., good astrometry), but hardly reliable for the measurement of the fireball speed. This is because the temporal data of the IMTN/CMN frames are not directly accessible from the commercial software used by IMTN/CMN operators. For this reason, the speed of the fireball was obtained from Rovigo data only. The timing data of a PRISMA station are easily accessible, and synchronization is made via NTP protocol, accuracy is not directly measurable, but it is better than 100 ms.

From the triangulations with the Rovigo station, we have excluded the Ferrara station because the angle value between the planes identified by these two stations is only 2.5°, too small to produce a reliable triangulation. The four possible 2-stations atmospheric trajectories are therefore given by Rovigo plane intersected with Casteggio/Confreria/Contigliano and Čiovo planes. The Rovigo–Casteggio and Rovigo–Contigliano trajectories are practically coincident (the difference is about 0.2 km on the ground), while between the other two remaining trajectories there is a difference of about 2 km if projected on the ground. The mean value of the two first trajectories provides the same parameters, but with less uncertainty, than the average of all the four trajectories. This makes the trajectory determined using the Borovička method between Rovigo, Casteggio and Contigliano the best trajectory, with the
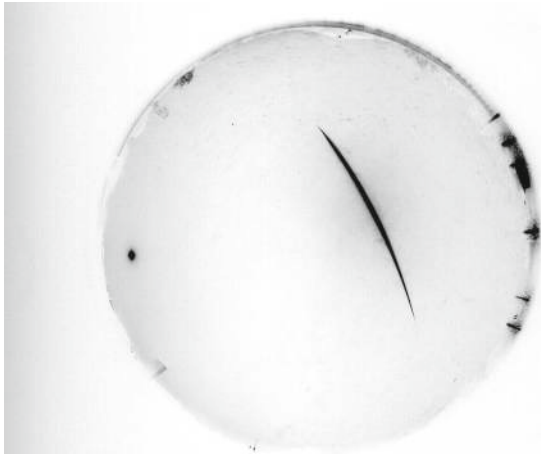
Fig. 3 A negative image showing the full path of IT20170530 from Rovigo. North is down; south is up. The bright object on the left is the Moon near the western horizons. The fireball moved from top left to bottom right. The total duration of the fireball was about 9.51 s. From this image, no significant fragmentation of the meteoroid appears

uncertainty computed as the mean observed deviation from the mean path (see Fig. 4 and Table 3).

The observed fireball path begins from a starting height $H_s = 81.1 \pm 0.2$ km and extinct at a terminal height $H_t = 23.3 \pm 0.2$ km, between the Italian cities of Venice and Padua. The total length of the luminous atmospheric path is about 115 km (Fig. 5). With these height values above sea level, the observed path was in a continuum flow regime and this affected the choice of the physical model to describe the fall of the meteoroid into the atmosphere [10].

The intersection between the fireball trajectory with the celestial sphere gives the apparent radiant position. Correcting it for the Earth's rotation and gravity (using "zenith attraction" method), we can compute the position of the true radiant [12]. The apparent radiant is in Virgo constellation and the true radiant in Hydra. The resulting values from triangulation are shown in Table 3. The rectangular geocentric coordinates x_i, y_i and z_i for every observed trajectory points are given directly by triangulation while the mean velocity between the observed points can be, as a first approximation, computed using the Pythagorean theorem:

$$v_i \approx \frac{\sqrt{(x_{i+1} - x_i)^2 + (y_{i+1} - y_i)^2 + (z_{i+1} - z_i)^2}}{(t_{i+1} - t_i)}. \tag{1}$$

However, this simple numerical approximation, given by Eq. (1), for the first derivative of the positions leads to more uncertainty which we reduced computing the central difference between data points. The central difference approximation is more accurate for smooth functions, as in our case. Things get worse if we compute the acceleration in the same kinematic way. However, it is important to know the speed instant by instant to trace the pre-atmospheric speed, before the entry of the meteoroid into the atmosphere, and the terminal speed that precedes the (possible), dark flight phase. So in order to compute the best height, velocity and acceleration (or mass–section ratio) in the terminal point of the luminous path, crucial parameters to the dark flight phase model, we have used a meteoroid single body dynamic model in a continuous flow regime to fit the observed data of
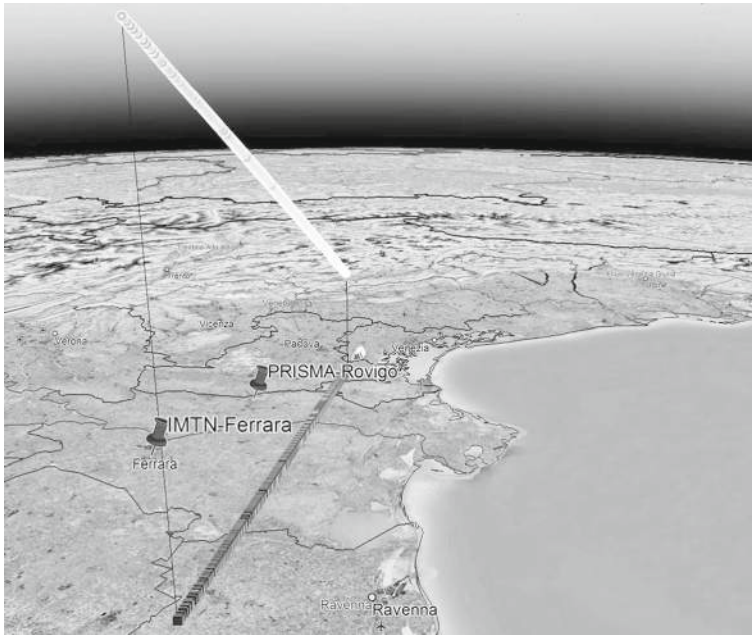
Fig. 4 A Google Earth map showing the best trajectories, both in atmosphere and projected on the ground, resulting from the triangulation between PRISMA-Rovigo, IMTN-Casteggio and IMTN-Contigliano

heights and speeds versus time. This model will be extensively discuss in the next section (Fig. 6).

5 The physical dynamic model of the meteoroid

In order to estimate the fireball main physical parameters, i.e., drag and ablation coefficients, pre-atmospheric velocity, mass/section ratio and to compute the best height, velocity and acceleration in the terminal point of the luminous path, we have used a single body dynamical model numerically integrating the differential equations describing the motion and the ablation of the meteoroid. In this classical model, no fragmentation is taken into account, but for our fireball no significant fragmentation of the meteoroid appears, see Fig. 3. Ablation begins when the surface of the meteoroid reaches the boiling temperature. At this point, the temperature is assumed to remain constant and the light emission negligible with respect to the kinetic energy of the meteoroid [10]. Under the hypothesis of a constant ablation rate and a constant body shape during its ablation, ours starting differential equations are as follows [22]:

$$\frac{\mathrm{d}v}{\mathrm{d}t} = -\frac{\Gamma \rho_a v^2}{D_\infty} \exp\left(-\frac{\sigma}{6}\left(v^2 - v_\infty{}^2\right)\right) \tag{2}$$

$$\frac{\mathrm{d}\rho_a}{\mathrm{d}t} = \frac{\rho_a v \cos z}{H} \tag{3}$$

$$\frac{\mathrm{d}h}{\mathrm{d}t} = -v \cos z \tag{4}$$

Table 3 Data about the starting/terminal points and the radiant (geocentric apparent and true), of the fireball trajectory from triangulations between PRISMA-Rovigo and IMTN-Casteggio/Contigliano stations

Quantity	Numerical value
H_s	81.1 ± 0.2 km
La_s (N, °)	44.369 ± 0.002 ($\pm$ 0.2 km)
Lo_s (E, °)	11.859 ± 0.002 ($\pm$ 0.2 km)
H_t	23.3 ± 0.2 km
La_t (N, °)	45.246 ± 0.002 ($\pm$ 0.2 km)
Lo_t (E, °)	12.046 ± 0.002 ($\pm$ 0.2 km)
T_i (°)	$30.8° \pm 0.1°$
A_z (from north to south, °)	$188.7° \pm 0.1°$
α_{GAR}^a (J2000.0)	$209.9° \pm 0.1°$
δ_{GAR}^a (J2000.0)	$-14.5° \pm 0.1°$
α_{GTR}^b (J2000.0)	$207.4° \pm 0.2°$
δ_{GTR}^b (J2000.0)	$-25.4° \pm 0.6°$

[a]*GAR* Geocentric Apparent Radiant
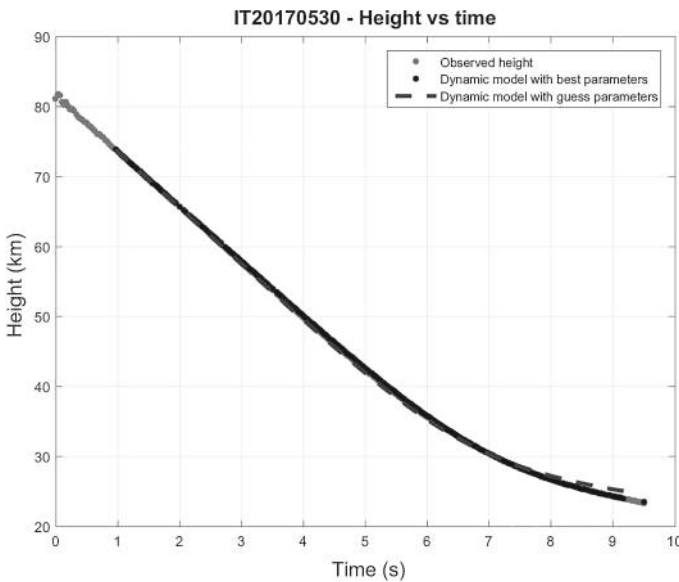[b]*GTR* Geocentric True Radiant

Fig. 5 Fireball height versus time as a result of the triangulation from Rovigo, Contigliano and Casteggio. Gray dots = observed values; dotted line = model with starting guess values; black line = best fit model

Equation (2) comes from the momentum–energy conservation, Eq. (3) is a consequence of the simple atmospheric density model adopted (i.e., the 1976 U. S. standard atmosphere model fitted with an exponential function), and Eq. (4) expresses a straight line model, i.e., we neglect the meteor curvature, which is a reasonable assumption for short trajectories of the order of about 100 km in length as in our case [21]. In the previous equations, the symbols have the meaning listed in Table 4.
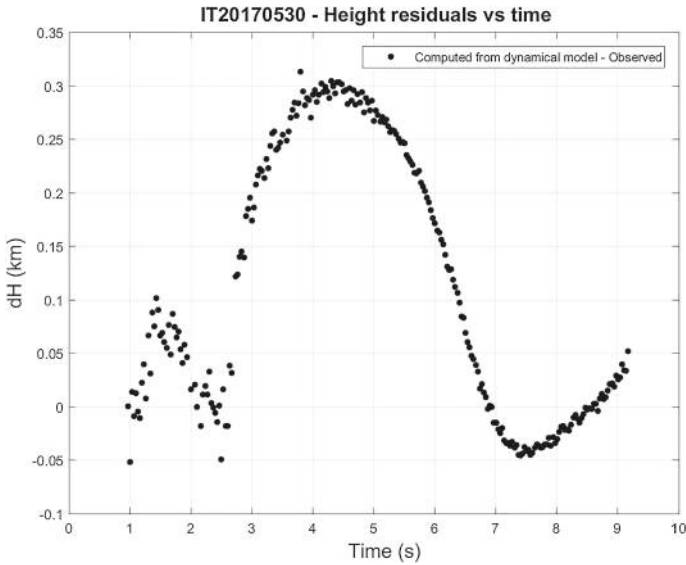
Fig. 6 Residual between the observed height versus time values and the dynamical model of the meteoroid (Rovigo, Contigliano and Casteggio). The mean residual value is about 0.12 km, discussion in the text

Table 4 Meaning of the symbols for Eqs. (2), (3) and (4)

Symbol	Quantity
v	Body speed with respect to the air
Γ	Aerodynamic drag coefficient
ρ_a	Air density (from 1976 US standard atmosphere model)
σ	Ablation coefficient
v_∞	Pre-atmospheric velocity
$D_\infty = m_\infty/A_\infty$	Pre-atmospheric mass–cross section ratio
z	Mean zenith distance of the fireball radiant
H	Effective atmosphere scale height (from 1976 US standard atmosphere model)

Note that the aerodynamic drag coefficient Γ is equal to $C_d/2$, where C_d is the usual drag coefficient used in fluid dynamics [22]. Numerically integrating the previous differential equations with Runge–Kutta fourth-/fifth-order methods and comparing the result with the observed values of $h(t)$ and $v(t)$, it was possible to estimate the best value of σ, v_∞ and D_∞ that fit the observed value starting from appropriate guess values. So we had performed a multi-parameter fitting using the observed data from trajectory and velocity together. The drag coefficient Γ has been kept fixed because, from Eq. (2), it is coupled to parameter D_∞
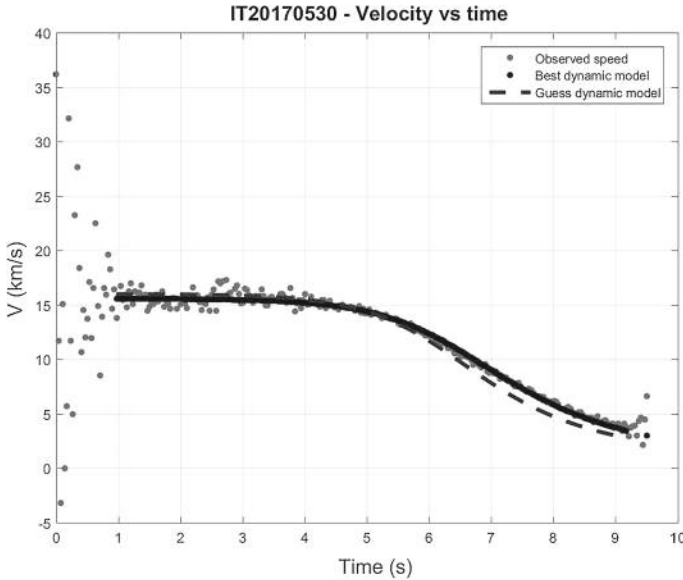
Fig. 7 Fireball velocity versus time as a result of the triangulation from Rovigo, Contigliano and Casteggio. The speed is computed using Rovigo's temporal data only. The initial dispersion of the points is due to the fact that the fireball was very far from the station and the displacement was low. In this condition, the sky position uncertainty is the dominant factor in the computed velocity. Gray dots = observed values; dotted black line = model with starting guess values; black line = best fit model

and cannot be determined separately. This choice weakly affects the subsequent dark flight phase because what matters is the Γ/D_∞ ratio (see Table 2).

As a starting value for the pre-atmospheric velocity, we have fitted the fireball observed velocity v versus the height h with the following exponential model from Ceplecha [11]:

$$v = v_\infty + c_v e^{(-bh)} \tag{5}$$

In this equation, c_v and b are constants to be determined together with v_∞. In general, these phenomenological models tend to be less accurate than the multi-parametric fit, but we only needed an estimate of the initial pre-atmospheric velocity [17]. Instead, as a starting value for D_∞, we have taken Eq. (2) computed with the estimated quantity in the terminal point of the luminous path:

$$D_\infty \approx \left(-\frac{\Gamma \rho_a v^2}{dv/dt} \right)_{\text{fin}} \exp\left(-\frac{\sigma}{6} \left(v_\infty{}^2 - v_{\text{fin}}{}^2 \right) \right) \tag{6}$$

In Eq. (6), the guess values of the fireball final velocity and the final acceleration are also estimated from the Ceplecha kinematic model [Eq. (5)]. We also have put $\sigma \approx 0.006 \, \text{s}^2/\text{km}^2$, the mean of the typical intrinsic ablation coefficient [14] and $\Gamma_{\text{fin}} = 0.58$ [12]. This last value for drag coefficient is equal to the starting value because we fixed Γ. In Sect. 6, we will see the effect of Γ variation on the dark flight phase.

In addition to the parameters that characterize the meteoroid, the solution of the differential equations of motion also depends by the starting height, speed and air density. Height and density values are well determined by observations and atmospheric model, respectively. The initial speed value V_{start} is more uncertain, see Fig. 7. As initial guess value of the meteoroid

Table 5 Values about the best fit parameter of the dynamic model, guess values and allowed variation range (Γ is keep fixed with a guess value equal to 0.58, as in [12]

Quantity	Best value	Guess value	Allowed range (min; max)
v_∞ (km/s)	15.9 ± 0.3	16.1	$v \pm 0.5$
σ (s^2/km^2)	0.0012 ± 0.0002	0.006	$\sigma/5; 5\sigma$
V_{start} (km/s)	15.6 ± 0.3	15.9	$V \pm 1$
D_∞ (kg/m^2)	234 ± 15	199	$D/5; 5D$
d_∞^{a} (m)	0.1		
m_∞^{b} (kg)	1.8		
D_{fin} (kg/m^2)	220 ± 10		
$d_{\text{fin}}^{\text{c}}$ (m)	0.09		
$m_{\text{fin}}^{\text{d}}$ (kg	1.6		
v_{fin}	3.0 ± 0.3 km/s		
a_{fin}	-1.19 km/s^2		
H_{fin}	23.4 ± 0.1 km		

In the last three rows of the table are the values of height, velocity and acceleration in the terminal point ($t = 9.51$ s), given by the model. Thanks to the low atmospheric speed, the meteoroid ablation was only partial and the model tells us that it is possible to find a small meteorite. Pay attention that the fireball physical model provides the Γ/D_∞ ratio only. The pre- and post-atmospheric mass and diameter values are guess assuming a mean density of about 3500 kg/m^3, i.e., a typical chondrite value, and a spherical shape. Their values are only indicative, not necessarily corresponding to the truth. Note that the σ value was blocked from the inferior boundary condition. If the range of variation is widened, the ablation value would become even smaller. It is not a software problem because the ablation values of the synthetic fireballs are correctly reproduced (see Table 2). Perhaps, this low ablation coefficient was simply due to a compact rock material
[a] pre-atmospheric diameter if chondrite
[b] pre-atmospheric mass if chondrite
[c] post-atmospheric diameter if chondrite
[d] post-atmospheric mass if chondrite

velocity, we took the one given by the Ceplecha model fit of the observed data (Eq. (5)). These initial guess values were allowed to vary in an appropriate physical range (see column 4 of Table 5).

After a least square fit of the $h(t)$ and $v(t)$ observed values, we obtained the results given in Table 5. The integration time starts 1 s after the fireball first detection from Rovigo and ends at 9.2 s, about 0.3 s before the end of the fireball path. In this way, we exclude the noisiest observed points from the numerical integration (see Fig. 7).

The initial guess values describe the first part of the trajectory very well, between 1 and 5 s, but not the last one (see Figs. 5, 7 and 9). So it is the second half of the trajectory that determines the best fit of the free parameters. The mean residuals are about 0.3 km/s for velocity and 0.1 km for height (see Figs. 6 and 8). In the height residuals, there is an evident systematic trend which remains confined within 0.3 km and is below 0.05 km near the terminal trajectory point: there are some height variations that the model cannot completely reproduce. The velocity trend appear better described although we can see a systematic effect between 5 and 8 s with an amplitude of about 0.3–0.4 km/s, about the order of magnitude of speed uncertainty. Assuming a mean density of about 3500 kg/m^3, we can estimate the mass and dimension of the meteoroid (see Table 5). With the dynamic model results, we can also compute a synthetic fireball light curve. Assuming that a fraction 0.04 of the meteoroid kinetic energy is converted into visible radiation, we found that the
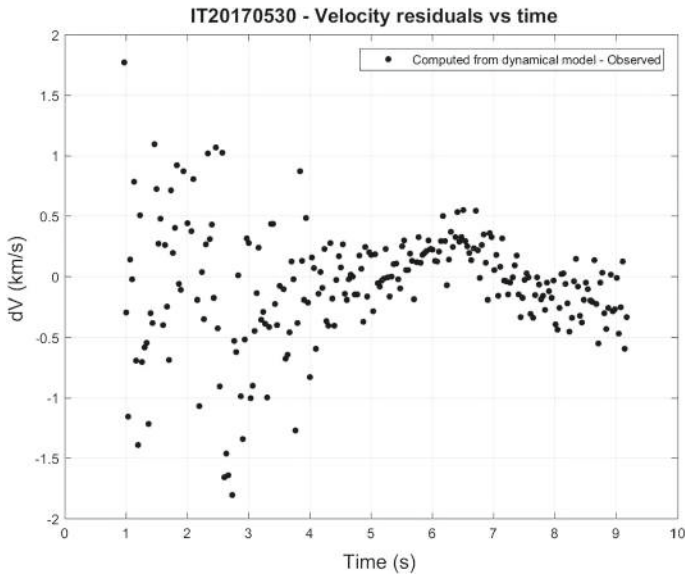
Fig. 8 Residual between the observed velocity values versus time and the dynamical model of the meteoroid (Rovigo with Contigliano and Casteggio). The mean residual value is about 0.3 km/s, discussion in the text

absolute magnitude reached a minimum of about -7.3 about 6.5 s after observation start [20]. This is a synthetic estimate of absolute magnitude at maximum brightness, so its value must be taken with caution. The computation of the absolute magnitude from Rovigo images is difficult because they are saturated and the values given by IMTN cameras are not reliable for the lack of the temporal data. The pre-atmospheric velocity is $v_\infty = 15.9 \pm 0.3$ km/s. Velocities of solar system meteoroids at their encounter with the Earth's atmosphere are within the following limits [13]: the lower one 11.2 km/s, if the meteoroid approaches the Earth from behind with zero relative velocity, and the upper one 72.8 km/s, if meteoroid strucks the Earth head-on. In this last case, we add the 42.5 km/s parabolic velocity at Earth's perihelion plus 30.3 km/s, the velocity of the Earth at perihelion. So the meteoroid belonged to the solar system. Correcting v_∞ for the attraction and the rotation of the Earth, we finally obtain the meteoroid geocentric velocity before entering the Earth's atmosphere [12]: $v_g = 11.4 \pm 0.4$ km/s. The corresponding heliocentric velocity is $v_g = 37 \pm 1$ km/s. In Sect. 8, knowing the position vector of the Earth at the fireball time, we will compute the meteoroid heliocentric osculating orbit.

6 The dark flight phase and the strewn field

In order to model the dark flight phase, it is important to know the profile of the atmosphere in the time and place closest to the meteoroid fall because the residual meteoroid trajectory, after the end of the luminous path, can be heavily influenced by the atmospheric conditions.

The data about wind velocity, wind direction, density, pressure and temperature versus the height above Earth's surface can be obtained from weather balloons up to an altitude of about 30–40 km. In Italy, there are eight weather stations for the sounding of the atmosphere that make balloons launches usually at 0 UT but also at 12 UT in case of adverse weather.

Table 6 Meaning of the symbols for Eqs. (7) and (8)

Symbol	Quantity
Γ	Aerodynamic drag coefficient
ρ_a	Fluid density
V	Fluid speed (in our case wind speed)
v	Body speed with respect to the fluid
v_c	Meteoroid speed with respect to the ground
A	Meteoroid cross section after the ablation phase
m	Meteoroid residual mass after the ablation phase
g	Standard acceleration due to gravity

Data from all stations over the world can be retrieved from the University of Wyoming Web site, Department of Atmospheric Science.[12] In our case, data from the weather stations 16080 LIML (Milano), 16045 LIPI (Rivolto) and 16144 San Pietro Capofiume were taken. All the weather data from these stations were taken at 0 UT of May 31, 2017, about 3 h after the fireball event. The nearest weather station to the terminal point of the luminous path was San Pietro Capofiume ($44°39'13.63''$ N; $11°37'22.28''$ E), about 100 km away. To compute the dark flight phase, we simply take these last atmospheric data without the use of an atmospheric model to propagate it in space and time. Later in the text, we will estimate how a change in the wind regime can influence the strewn field center.

The motion of the residual meteoroid, starting from the observed terminal point of the luminous path, can be described using Newton's Resistance law as in Ceplecha [12], because the meteoroid motion takes place in a turbulent regime, i.e., a motion characterized by high Reynolds number (see below), and the gravity force law. In gas dynamics physics, the full vector equation of the meteoroid motion during dark flight is as follows:

$$\boldsymbol{a} = -\Gamma \rho_a v \frac{A}{m} \boldsymbol{v} + \boldsymbol{g} \tag{7}$$

with

$$\boldsymbol{v} = \boldsymbol{v}_c - \boldsymbol{V} \tag{8}$$

In the previous equations, the symbols have the meaning listed in Table 6. Making the substitution:

$$\boldsymbol{a} = \frac{\mathrm{d}\boldsymbol{v}}{\mathrm{d}t} = \frac{\mathrm{d}\boldsymbol{v}}{\mathrm{d}h}\frac{\mathrm{d}h}{\mathrm{d}t} = \frac{\mathrm{d}\boldsymbol{v}}{\mathrm{d}h}v_h \tag{9}$$

Equation (7) takes the form:

$$\frac{\mathrm{d}\boldsymbol{v}}{\mathrm{d}h} = -\frac{1}{v_h}\Gamma \rho_a v \frac{A}{m} \boldsymbol{v} + \frac{\boldsymbol{g}}{v_h} = -\frac{\Gamma \rho_a v}{D_{\mathrm{fin}} v_h} \boldsymbol{v} + \frac{\boldsymbol{g}}{v_h} \tag{10}$$

To apply Eq. (10) in the real world, it is assumed that ablation suddenly stops after the last observation was made. This may not be strictly true as the final point of the fireball trajectory could be just due to the observation range or to the sensitivity of the sensor that prevents from seeing the full fireball trajectory. Considering that the Rovigo station was very close to the terminal point of the fireball's trajectory (about 36 km), this effect is supposed to be not very important here (Figs. 9, 10).

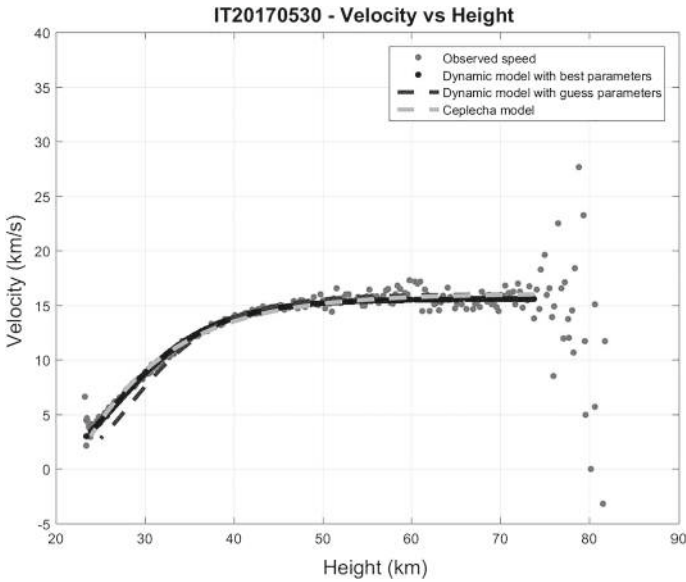[12] http://weather.uwyo.edu/upperair/sounding.html.

Fig. 9 Fireball velocity versus height as a result of the triangulation from Rovigo with Contigliano and Casteggio. Gray dots = observed values; dotted black line = model with starting guess values; black line = best fit model
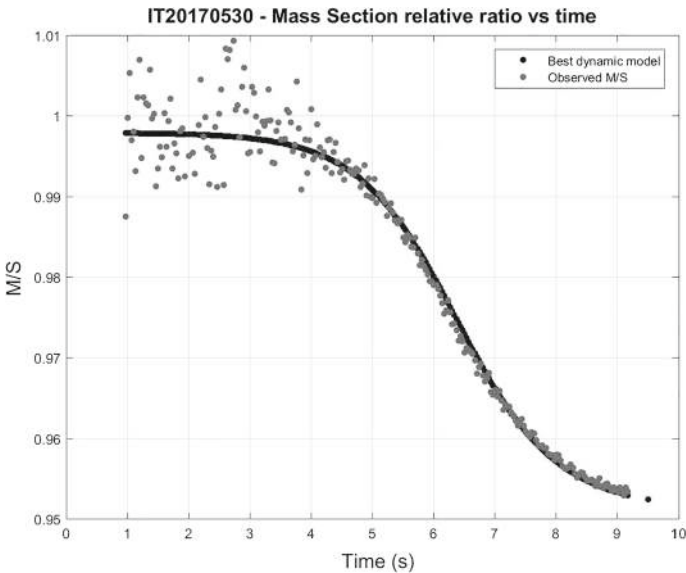

Fig. 10 Fireball relative mass/(cross section) ratio versus time as a result of the triangulation from Rovigo with Contigliano and Casteggio. In this figure, it is possible to follow the meteoroid ablation versus time because $M/S \propto r$, where r is the meteoroid radius. The best fit model line starts below 1 because the first observation was made when the ablation was already on. The scattering is due to the initial uncertainty on the fireball speed. Gray dots = observed values; black line = best fit model
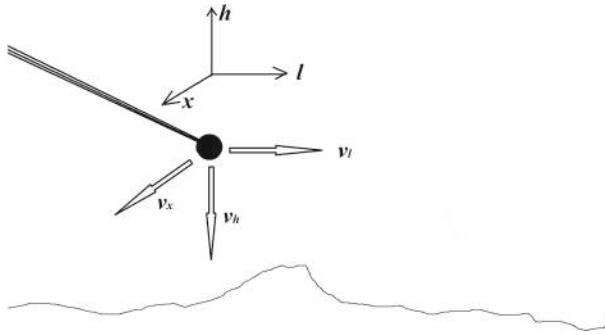
Fig. 11 Fireball reference system (l, h, x) for dark flight phase. The black dot is the terminal point of the luminous path. The component velocity v_l is parallel to the fireball motion direction, v_x is along the orthogonal direction, and v_h is toward the bottom (so $v_h < 0$ always)
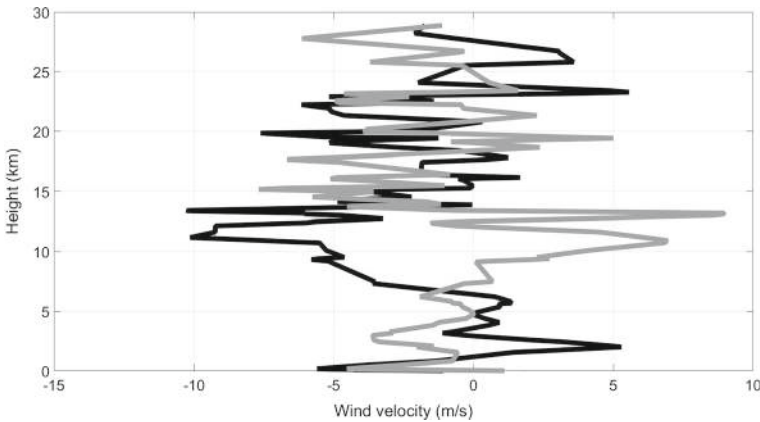

Fig. 12 Wind speed versus height in the meteoroid reference system from San Pietro Capofiume. Black line: wind along meteoroid motion direction (l axis). Wind speed values greater than zero are against meteoroid motion. Gray line: right orthogonal direction to the meteoroid motion (l_x axis). Wind speed values greater than zero are against the positive direction of v_x

Ceplecha also takes into account Coriolis force, even if it is a small contribution and it is not shown in the previous equations [12]. In our numerical computations, we also include the Earth's rotation. The reference system of the previous motion equations is shown in Fig. 11. The origin of this reference system is in the terminal point of the fireball path. Numerically integrating this differential equation with the winds values shown in Fig. 12, we directly obtain meteoroid velocity versus height above the ground.

The ratio $m/A = D_{\text{fin}}$ and the Γ value are given by the dynamical model of the previous section. The value of the aerodynamic drag coefficient Γ depends both on the unknown final form of the meteoroid after ablation, on the Reynolds number and on the Mach number, i.e., the ratio between the meteoroid speed and the sound speed at the same height above ground. Assuming, for the residual meteoroid, a diameter d of about 0.1 m (Table 5), and taking into account air density and temperature in the terminal point of the fireball, a Reynolds number $\text{Re} = \rho v d/\mu \approx 10^6$ can be estimated (μ is the dynamic viscosity of the fluid). That is, we are in a turbulent regime and this justifies resort to Newton's Resistance law. The same Reynolds number still holds when the residual meteoroid touches the ground, because the

Table 7 Data regarding the impact points with different m/A final values compatible with the uncertainty given in Table 5

Quantity			
Final m/A (kg/m^2)	210	220	230
Lat. N impact point (°)	45.3522	45.3546	45.3570
Long. E impact point (°)	12.0705	12.0710	12.0715
L (km)	11.9	12.2	12.5
v_{impact} (m/s)	74	76	78

decrease in speed is roughly compensated by the increase in air density (see Table 7). In general—with Mach number between 8 and 20—for a spherical body the drag coefficient Γ decreases with the increase in the Reynolds number toward an asymptotic value near 0.3–0.4 for $R_e > 10^4$ [2]. The value of the drag coefficient Γ is independent of the size, the crucial parameter being the body shape. In our case, the residual meteoroid will not be a perfect sphere so it is reasonable to expect that the Γ values are a bit higher toward high Mach and Reynolds numbers.

For the asymptotic value, i.e., toward very high Mach numbers (Reynolds number is always high), the value $\Gamma = 0.58$, that we fix in the meteoroid dynamic model, appears reasonable. For low Mach numbers instead, i.e., equal or less than 4, we adopt the Ceplecha's values [12]: $\Gamma(4) = 0.58$, $\Gamma(3) = 0.62$, $\Gamma(2) = 0.63$, $\Gamma(1) = 0.50$, $\Gamma(0.8) = 0.44$, $\Gamma(0.6) = 0.39$, $\Gamma(0.4) = 0.35$ and $\Gamma(0.2) = 0.33$. Finally, the horizontal distance along the l axis, between the terminal point projected on the ground and the impact point, is given by:

$$L = \int_0^T v_l \, \mathrm{d}t = \int_{h_T}^{h_S} v_l \frac{\mathrm{d}h}{v_h} \Rightarrow L = \int_{h_S}^{h_T} v_l \frac{\mathrm{d}h}{v_h} \text{ with } v_h > 0 \tag{11}$$

A similar equation holds for L_x, the orthogonal displacement [12]. These distances, L and L_x, were computed with numerical integration of the motion equations assuming, as starting conditions, the position, velocity and acceleration given in Table 5 with the dynamical model computed at the terminal point of the fireball (see Figs. 13 and 14).

From our computation, we found that the Mach number in the terminal point of the fireball phase is about 10. Mach numbers fall below 4 only in the last 20 km above the ground. To demarcate the probable impact zone, we have chosen three different values for the m/A ratio in the terminal point (see Table 7), according with the uncertainty given in Table 5, and seen how different impact points are distributed on the ground. According to the m/A values, the distance of the impact point from the projection on the ground of the terminal point varies from 11.9 to 12.5 km with a difference of about 0.6 km. The impact velocity with the ground is around 76 m/s, i.e., about 274 km/h. The uncertainty about velocity and height in the terminal point have a minor influence over the impact point. We have delimited the full strewn field using a Monte Carlo simulation, i.e., creating 1000 virtual meteoroids with parameters compatible with the observations in the terminal point and computing for each of them the point of fall. The full strewn field has an extension of about 1.7×0.6 km (see Fig. 15).

Considering that we used weather data 100 km away in space and 3 h in time from the place and instant of the fireball fall, the weak point of these results about the strewn field is that the assumed wind regime probably is not similar to that really present during the fall. So we have made a rough estimate of how important is to know the exact atmospheric state to compute the strewn field. We recompute the dark flight using the data from the weather stations 16080 (Milano, 250 km away), 16045 (Rivolto, 100 km away) and 16144 (Capofiume), both for 0
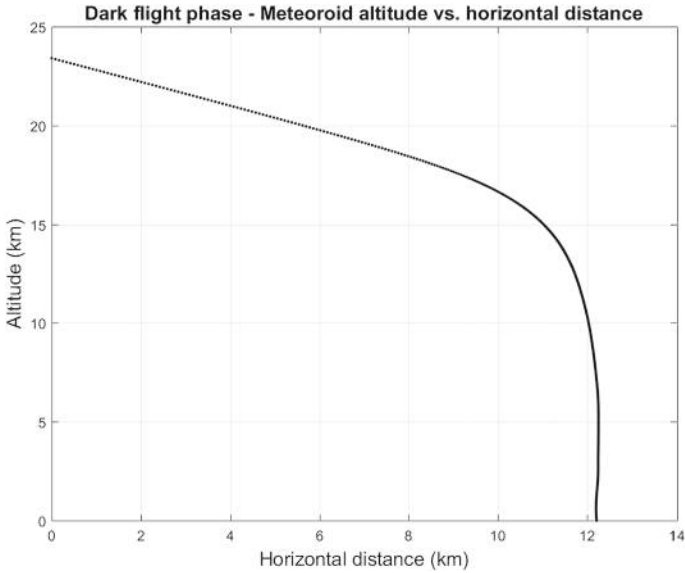
Fig. 13 Parallel view of the residual meteoroid height versus horizontal distance along the l axis starting from the terminal point. Notice the small deformations at the end of the vertical section of the trajectory, due to the wind

Fig. 14 Front view of the residual meteoroid trajectory. Meteoroid height versus orthogonal distance l_x. The trajectory oscillations are in phase with the winds directions, but the orthogonal movements are a few tens of meters only

Fig. 15 A Google Earth maps showing the possible impact points on the ground obtained from the Monte Carlo simulation. The strewn field dimension is about 1.7×0.6 km, about north of the town of Bojon

UT of May 30 and 31. The result is that the six nominal impact points are very close, with a standard deviation of about 0.5 km in latitude and 0.4 km in longitude. So it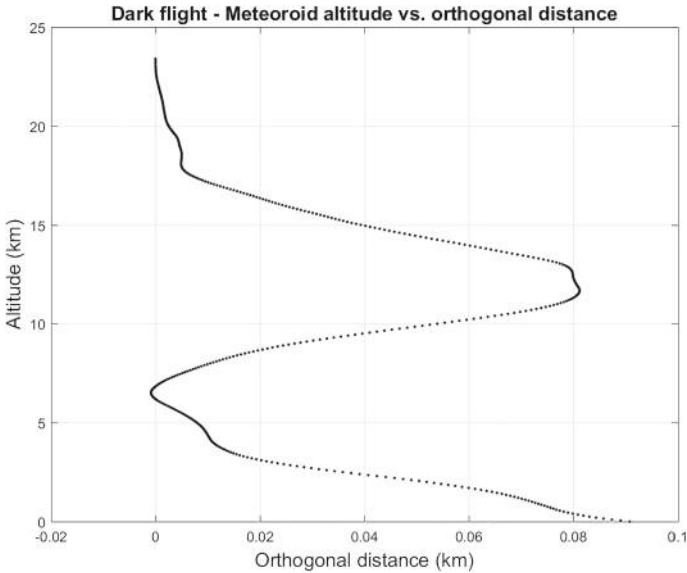 can be expected that the change in wind speed has shifted the nominal impact point by about 0.6 km in any direction. For future interesting fireballs, it will be desirable to use atmospheric models to obtain the wind regime and the state of the atmosphere for the desired place and time in order to reduce strewn field uncertainty.

7 In search for meteorites

After numerical computation of the possible impact points on the ground, we looked for meteorites. Immediately, after the fall the strewn field was wider than indicated in this paper, because the speed at the end point was estimated with simple kinematic considerations. Only after introducing the dynamic model for the meteoroid was the search area better delimited.

Public appeals have been made to the population of the areas involved, including on the PRISMA Web site[13] in several newspapers as well as on social media. Following these appeals, over ten suspected meteorites have been collected by local inhabitants. The samples have been all identified as common ground stones. We also did directly search the predicted strewn field starting a few days after the fall until the early July 2017, and a second search was done in April 2018. A great contribution for meteorites search came from "Meteoriti Italia," a group of amateur meteorite enthusiasts who like to support researchers, contributed greatly by assisting on the meteorite search trips. Unfortunately, the area where the "on field research" took place is densely populated and settled with villages, streets and water

---

[13] http://www.prisma.inaf.it/index.php/2017/06/27/bolide-del-30-maggio-era-un-mini-asteroide-segnalate ci-eventuali-sassi-strani-o-anomali/.

channels. Moreover, it is also a place of an intensive agricultural activity. There were several crops in progress, including wheat fields, that could not be accessed until after harvest. This "difficult territory" has hindered searches, and no meteorites were found. The only collected objects, at first sight similar to a meteorite, were some rounded fragments of black volcanic glass. Probably, the glass originated from the ancient volcanoes that gave origin to a hills site called "Colli Euganei" about 30 million years ago [24], and located about 30 km away from the computed impact points. However, we do not rule out the possibility to find a meteorite in a near future with more thorough searches.

8 The meteoroid heliocentric orbit and the search for a progenitor body

Knowing the heliocentric velocity vector of the progenitor meteoroid and the Earth's vector position at the time of the meteoroid fall, it is possible to compute the heliocentric orbital elements [12,26]. As to our case, it is interesting to note that a comparison between Ceplecha analytical orbit determination method and numerical integration yields consistent results [16].

Of course, uncertainty about the heliocentric speed, both in length and direction, also makes the orbital elements uncertain (see Table 8 and Fig. 16). In order to estimate the uncertainty of the orbital elements, a Monte Carlo approach with 100 clones was performed. The computed orbital elements indicate that the meteoroid was an Apollo-type object, with an aphelion near the outer Main Belt and with low inclination above the Ecliptic plane. With the data from Table 8, the heliocentric distance of the ascending node was about 1.022 UA, whereas the descending node was near 2.81 AU. Incidentally, we note that the heliocentric distance of the ascending node is consistent with that of the Earth on May 30, 2017, i.e., 1.014 AU.

In order to identify a possible parent body among the known NEAs, we use the D_N criterion introduced by [27] for meteoroid stream identification:

$$D_N = \sqrt{(U - U_0)^2 + (\cos\theta - \cos\theta_0)^2 + \left(2\sin\frac{\phi - \phi_0}{2}\right)^2 + \left(2\sin\frac{\lambda - \lambda_\oplus}{2}\right)^2} \quad (12)$$

At variance with most other criteria, based on the heliocentric orbital elements, this criterion uses geocentric quantities and two of the quantities that are used in D_N (i.e., U and $cos\theta$) have been shown to be nearly invariant under the secular perturbation. Many factors influence the dynamical evolution of a meteoroid, and some of them result from forces other than gravitation, especially for meteoroids of very small size. However, over not too long time scales, and in the absence of planetary close encounters, we can assume that only planetary secular perturbations affect meteoroid orbits. For this reason, we consider the D_N criterion useful for finding a progenitor. We refer the reader to [27] for the details and to [18] and [23] for comparisons with other criteria.

For the NEAs, the relevant quantities are conveniently tabulated by NEODyS[14]; for IT20170530 we have $U_0 = 0.38 \pm 0.02$, $\theta_0 = 56.0° \pm 0.2°$, $\phi_0 = 286° \pm 0.7°$ and $\lambda_\oplus = 249.4°$ (the longitude of the Earth at the time of fall).

Table 9 reports the NEAs characterized by $D_N < 0.15$ with respect to IT20170530; the same NEAs are shown in the U-$\cos\theta$ plane in Fig. 17. Practically, all of these NEAs are small to very small objects, characterized by very low values of their MOID (Minimum Orbit Intersection Distance); the exception is (523,685) 2014 DN_{112}, a numbered object

---

[14] https://newton.spacedys.com/~neodys2/propneo/encounter.cond.

Table 8 Data about the meteoroid heliocentric orbit

Quantity	Numerical value
Semi major axis (AU)	2.3 ± 0.2
Eccentricity	0.59 ± 0.03
Orbital period (years)	3.4 ± 0.4
Orbit inclination (°)	4.2 ± 0.1
Longitude of the ascending node (°)	249.4002 ± 0.0001
Argument of Perihelion (°)	37.7 ± 0.1
Perihelion passage (JD)	2456672.9 ± 138
Perihelion distance (AU)	0.94 ± 0.01
Aphelion distance (AU)	3.6 ± 0.3

The standard deviations are obtained with a Monte Carlo computation over 100 clones. The longitude of the ascending node has very low uncertainty because the value is only determined by the time of the fireball fall
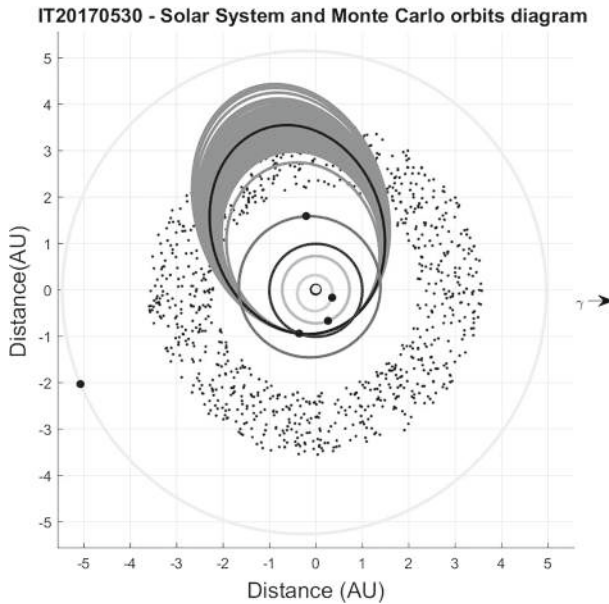
Fig. 16 Nominal heliocentric orbit for the progenitor meteoroid of the fireball IT20170530 as seen from the ecliptic north pole. The dots symbolically represent the Main Belt. The position of the planets on their orbits is that at the time of the fireball. The fireball clones orbit are indicated in gray color

characterized by $H = 20.0$. However, none of the orbits of the NEAs in the table is particularly close to the orbit of the fireball. However, Fig. 17 and Table 9 show that the meteoroid was in a region populated by small NEAs, which suggests a possible asteroidal origin. We plan to continue to scan the NEAs database to see if new asteroids, with lower D_N values, will be discovered.

Fig. 17 Black dots show the NEAs with $D_N < 0.15$ in the plane U-$\cos\theta$; the big red dot shows IT20170530. The region below the $a = \infty$ line contains orbits bound to the Sun, and the region on the left of the $i = 90°$ line contains prograde orbits
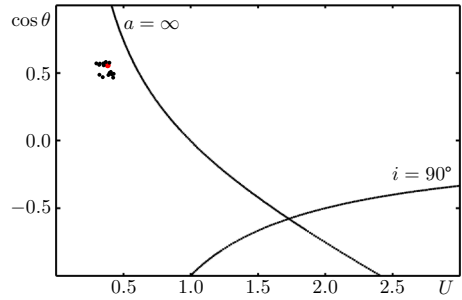
Table 9 NEAs with geocentric parameters U, θ, ϕ and λ close to the IT20170530 values

	NEA	U	$\theta(°)$	$\phi(°)$	$\lambda(°)$	D_N
	2011 UR$_{63}$	0.40	60°0	285°3	251°3	0.067
	2017 WD	0.35	55°9	285°5	254°7	0.072
	2018 VL$_3$	0.39	54°7	280°6	255°3	0.101
	2008 TQ$_{26}$	0.34	61°9	288°3	245°3	0.112
	2017 WO$_{13}$	0.39	59°8	278°3	248°1	0.113
	2018 WT$_1$	0.32	55°1	291°3	242°1	0.126
	2019 EU	0.35	55°0	289°5	259°1	0.132
	2017 KW$_4$	0.42	62°1	292°4	246°5	0.132
	2017 PL$_{26}$	0.30	54°9	280°2	255°3	0.134
	2017 KR$_{27}$	0.41	60°5	290°6	241°0	0.139
	2011 UD$_{115}$	0.32	60°7	293°8	245°8	0.141
	2012 VT$_{76}$	0.39	60°8	277°5	254°6	0.143
	2011 PO$_1$	0.42	60°3	282°7	258°8	0.146
	2005 XO$_4$	0.37	54°3	277°5	257°8	0.149
(523,685)	2014 DN$_{112}$	0.32	55°7	289°5	239°0	0.149
	1997 UA$_{11}$	0.40	59°4	281°4	239°1	0.150
		U	θ	ϕ	$\lambda_\oplus$	
IT20170530		0.38	56°0	286°0	249°4	

The uncertainty on the asteroids elements is one or more orders of magnitude lower than that of the meteoroid

9 Conclusions

We have presented the main results about the fireball IT20170530, observed by PRISMA, IMTN and CMN stations on May 30, 2017, at about 21h 09m 17s UTC. Unfortunately, only data from the Rovigo station appear to be the most complete and usable, which represented a significant shortcoming in the analysis. However, according to our results, the progenitor meteoroid entered the atmosphere at a speed $v_\infty = 15.9 \pm 0.3$ km/s, with an estimated starting mass/section ratio $D_\infty = 234 \pm 15$ kg/m^2. If the body was a spherical chondrite with mean drag coefficient $\Gamma = 0.58$, we estimated a guess starting diameter of about 0.1 m and a mass of about 1.8 kg. Thanks to the low relative speed with the Earth, the ablation was slow and the dynamic model indicates that a residual meteoroid is possible because $D_{\text{fin}} > 0$.

The fireball path extinct at a terminal height $H_t = 23.3 \pm 0.2$ km (Lat. $45.246° \pm 0.002°$ N; Long. $12.046° \pm 0.002°$ E) between the Italian cities of Venice and Padua. The dark flight phase led the residual meteoroid, of about 0.09 m diameter and mass 1.6 kg (guess values), to fall about 11.9–12.5 km beyond the trajectory terminal point. The effect of the winds and wind variation on the fall was several hundred of meters at most. Also important is the effect of the final mass–cross section ratio uncertainty that has led us to delimit a minimum strewn field of about 1.7×0.6 km. In this and a larger area, we searched unsuccessfully for meteorites. The progenitor meteoroid heliocentric orbit indicates that the body came from the outer Main Belt of asteroids, but it is uncertain because the speed values come from the Rovigo station only. The search for a specific progenitor body among the known NEAs has not given good candidates, but we plan to continue to scan the NEAs database to see if new asteroids, with lower D_N values, will be discovered.

The physical analysis of the fireballs set out in this paper will serve as a reference for future events. Thanks to the great expansion of PRISMA network in Italy, we hope to have interesting events whose data come only from PRISMA stations, in order to have maximum data homogeneity. In the case of IT20170530, having non-homogeneous data certainly was not good, for example as regards the measure of speed versus time. The lack of usable photometric data concerns only this specific case; we hope to be able to obtain the light curves of the fireballs from the PRISMA cameras far enough away that they are not saturated.

The implementation of an automatic pipeline for PRISMA is in progress. It would be necessary to have a real-time alert system which, depending on the fireball final height, warns if the fireball extinguishes below 25–30 km from ground. These are the events where meteorites are most likely. An automatic alert system would allow us to arrive as soon as possible to look for the meteorite in the strewn field, minimizing terrestrial contamination. In this case, no meteorites were found, but it happened with the very recent fireball IT20200101 at 18:26:54 UT. This historic event will be the subject of a next paper.

References

1. Y. Audureau, C. Marmo, S. Bouley, M. K. Kwon, F. Colas, J. Vaubaillon, M. Birlan, B. Zanda, P. Vernazza, S. Caminade, J. Gattacceca, IMO, in *Proceedings of the 2014 International Meteor Conference*, pp. 39–41 (2015)
2. A.B. Bailey, J. Hiatt, A.E.D.C. Tech. Rep. 70-291 (1971)
3. M. Beech, P. Brown, R.L. Hawkes, Z. Ceplecha, K. Mossman, G. Wetherill, Earth Moon Planets **68**, 189–197 (1995)
4. A. Bertin, ASP Conf. Ser. **351**, 112 (2006)
5. E. Bertin, S. Arnouts, Astron. Astrophys. Suppl. **117**, 393–404 (1996)
6. D. Barghini, D. Gardiol, A. Carbognani, S. Mancuso, Astron. Astrophys. **626**, A105 (2019)
7. J. Borovička, Bull. Astron. Inst. Czechoslov. **41**, 391–396 (1990)
8. J. Borovička, Publication of the Astronomical Institute of the Czechoslovak Academy of Sciences **79** (1992)
9. J. Borovička, P. Spurny, J. Keclikova, Astron. Astrophys. Suppl. Ser. **112**, 173–178 (1995)
10. M.D. Campbell-Brown, D. Koschny, Astron. Astrophys. **418**, 751–758 (2004)
11. Z. Ceplecha, Bull. Astron. Inst. Czechoslov. **2**, 21–47 (1961)

12. Z. Ceplecha, Bull. Astron. Inst. Czechoslov. **38**, 222–234 (1987)
13. Z. Ceplecha, J. Borovicka, W.G. Elford, D.O. Revelle, R.L. Hawkes, V. Porubcan, M. Šimek, Space Sci. Rev. **84**, 327–471 (1998)
14. Z. Ceplecha, D.O. ReVelle, Meteorit. Planet. Sci. **40**, 35–54 (2005)
15. F. Colas, et al., European Planetary Science Congress 2015, 10, EPSC2015-800 (2015)
16. D.L. Clark, P.A. Wiegert, Meteorit. Planet. Sci. **46**, 1217–1225 (2011)
17. A. Egal, P.S. Gural, J. Vaubaillon, F. Colas, W. Thuillot, Icarus **294**, 43–57 (2017)
18. D.P. Galligan, Mon. Not. R. Astron. Soc. **327**, 623–628 (2001)
19. D. Gardiol, A. Cellino, M. Di Martino, *Proceedings of the International Meteor Conference* (Egmond, Netherlands, 2016), pp. 76–79
20. M. Gritsevich, D. Koschny, Icarus **212**, 877–884 (2011)
21. S. Jeanne et al., Astron. Astrophys. **627**, A78 (2019)
22. V.V. Kalenichenko, Astron. Astrophys. **448**, 1185–1190 (2006)
23. A.V. Moorhead, Mon. Not. R. Astron. Soc. **455**, 4329–4338 (2016)
24. G. Piccoli, R. Sedea, R. Bellati, E. Di Lallo, F. Medizza, A. Girardi, R. De Pieri, G.P. De Vecchi, A. Gregnanin, E.M. Piccirillo, A. Norinelli, A. Dal Pra, Memorie degli Istituti di Geologia e Mineralogia dell'Univ. di Padova, 34, 523–566 (1981)
25. O.P. Popova et al., Science **342**(6162), 1069–1073 (2013)
26. T.E. Sterne, *An Introduction to Celestial Mechanics* (Interscience Publishers, New York, 1960), p. 206
27. G.B. Valsecchi, T.J. Jopek, Froeschlé Cl, Mon. Not. R. Astron. Soc. **304**, 743–750 (1999)